Langmuir

Article

pubs.acs.org/Langmuir

Poly(ethylene glycol)-Based Multidentate Oligomers for Biocompatible Semiconductor and Gold Nanocrystals

Goutam Palui, Hyon Bin Na, and Hedi Mattoussi*

Department of Chemistry and Biochemistry, Florida State University, 95 Chieftan Way, Tallahassee, Florida 32306, United States

Supporting Information

ABSTRACT: We have developed a new set of multifunctional multidentate OligoPEG ligands, each containing a central oligomer on which were laterally grafted several short poly(ethylene glycol) (PEG) moieties appended with either thioctic acid (TA) or terminally reactive groups. Reduction of the TAs (e.g., in the presence of $NaBH_4$) provides dihydrolipoic acid (DHLA)-appended oligomers. Here the insertion of PEG segments in the ligand structure promotes water solubility and reduces nonspecific interactions, while TA and DHLA groups provide multidentate anchoring onto Au nanoparticles (AuNPs) and ZnS-overcoated semiconductor quantum dots (QDs), respectively. The synthetic route involves simple coupling chemistry using *N*,*N*-dicylohexylcarbodiimide (DCC). Water-soluble QDs and AuNPs capped with these ligands were prepared via cap exchange. As prepared, the nanocrystals dispersions were aggregation-free, homogeneous, and stable for extended periods of time over pH ranging from 2 to 14 and in the presence of excess electrolyte (2 M NaCl). The new OligoPEG ligands also allow easy integration of tunable functional and reactive groups within their structures (e.g., azide or amine), which imparts surface functionalities to the nanocrystals and opens up the possibility of bioconjugation with specific biological molecules. The improved colloidal stability combined with reactivity offer the possibility of using the nanocrystals as biological probes in an array of complex and biologically relevant media.

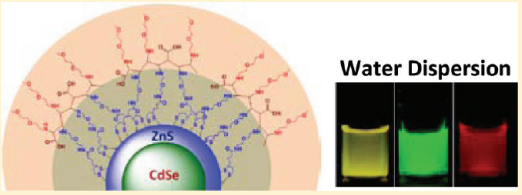

INTRODUCTION

Inorganic nanocrystals such as semiconductor quantum dots (QDs) and gold nanoparticles (AuNPs) are excellent and promising candidates for use in developing an array of applications ranging from electronic devices[1,2] to lasers,[3,4] photovoltaic cells,[5,6] analytical sensors,[7,8] and biomedical imaging.[9−13] This potential stems from some of their unique physical and chemical properties that often exhibit size and composition dependence. Semiconductor nanocrystals such as those made of CdSe, CdS, and InAs cores have tunable size-dependent broad absorption, with very high extinction coefficients, and size-dependent narrow Gaussian emission profiles, which are not easily available with conventional organic fluorophores and fluorescent proteins;[2,9,10,13] CdSe-based nanocrystals, in particular, were shown to exhibit remarkable resistance to chemical and photodegradation.[9,14,15] These features have generated a great interest for developing QDs as fluorescent platforms for use in biotechnology.[9−16] Such platforms promise great advances in understanding a variety of biological processes, ranging from sensing to the tracking of intracellular protein movements and interactions. Successful integration in biotechnology requires the preparation of robust, water dispersible QDs that exhibit long-term stability over a wide range of biological conditions. It also requires that the resulting nanocrystals be compatible with simple bioconjugation techniques in order to allow straightforward and controllable coupling to biomolecules such as proteins, peptides and DNAs.

Over the last 3 decades, three chemical approaches have been employed to synthesize luminescent QDs: (1) growth in inverse micelles (aqueous) carried at room temperature,[17,18] (2) pyrolysis of organometallic precursors at high temperature and in coordinating solution,[19−21] and (3) arrested precipitation carried out in aqueous solution using hydrophilic ligands such as thioglycolic acid.[22,23] QDs grown at high temperature exhibit better physical characteristics, namely, narrow size distribution and crystalline cores, along with superior optical and spectroscopic properties and high fluorescence quantum yields.[19−21,24−26] As made these QDs are capped with hydrophobic ligands and thus are dispersible only in organic solutions. Postsynthetic surface modification is required to render the nanocrystals soluble in buffer media and compatible with biological conditions.

Gold nanoparticles are often prepared using the classic citrate reduction of aurate pioneered by Turkevich et al. and Frens.[27,28] This synthesis route provides citrate-stabilized nanoparticles, and these too require surface modification with appropriate hydrophilic ligands if further conjugation to biomolecules is desired.

A few strategies have been applied in the past decade to promote the transfer of QDs to buffer media, including silica coating,[29−31] encapsulation within amphiphilic polymers and phospholipid micelles,[32−38] and exchanging the native hydro-

Received: October 10, 2011
Revised: December 9, 2011
Published: December 27, 2011

   dx.doi.org/10.1021/la203968t | Langmuir 2012, 28, 2761−2772

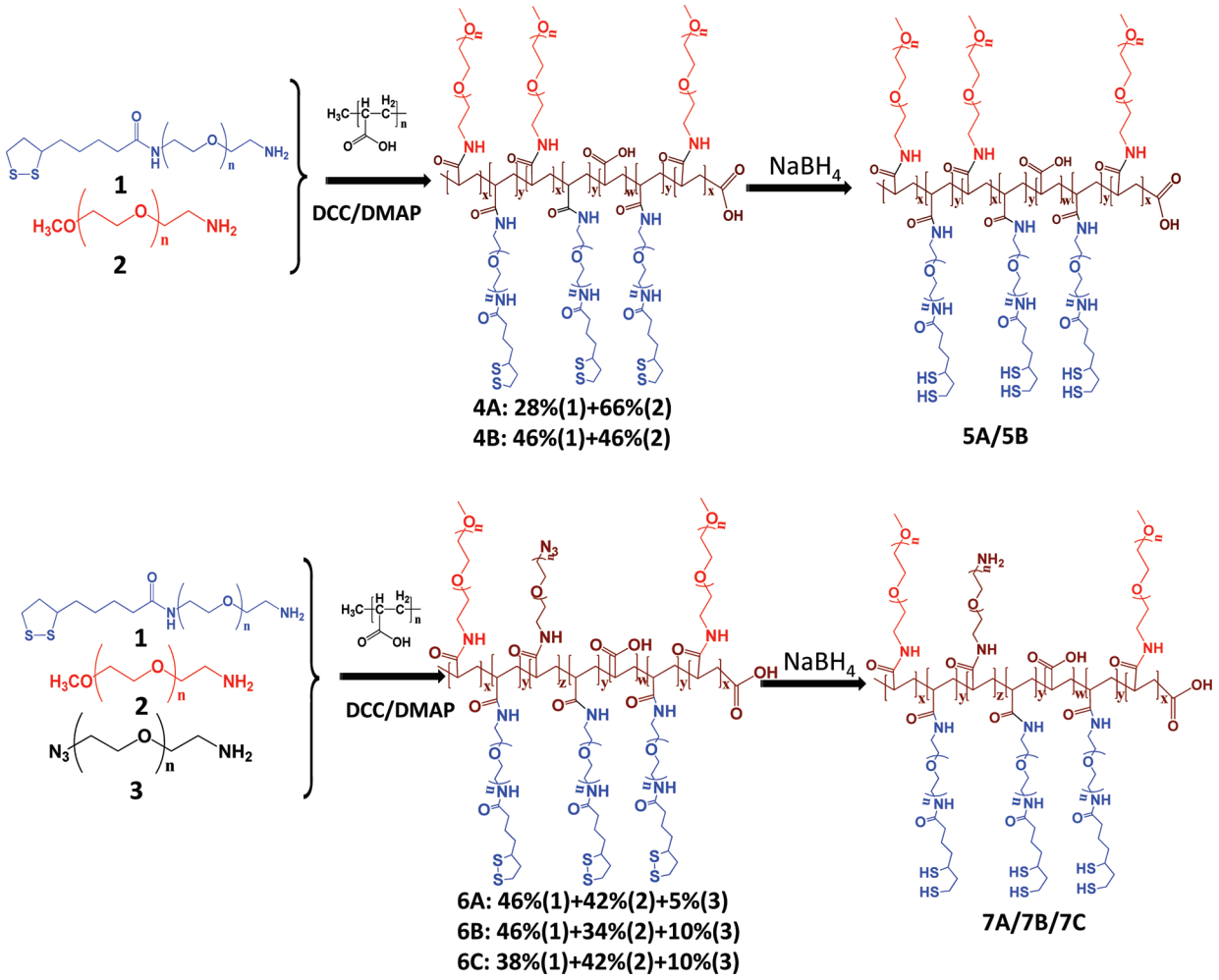

Figure 1. Chemical structures and synthetic strategy of the poly(ethylene glycol)-grafted-poly(acrylic acid), OligoPEG ligands. *x*, *y*, *z*, and *w* designate the relative abundance of methoxy-PEG, TA/DHLA–PEG, N_3/NH_2–PEG, and unreacted carboxyl along the PAA chain. DCC: *N*,*N*-dicylohexylcarbodiimide; DMAP: 4-dimethylamino-pyridine.

phobic cap with hydrophilic organic ligands.[39−43] Cap exchange with bifunctional ligands has found wider use because it is relatively easy to implement and it tends to produce compact nanocrystals;[39−42] small hydrodynamic size nanocrystals are needed. Regardless of the strategy used, a few key properties of the hydrophilic nanocrystals are highly desired. These include colloidal stability of the nanocrystals over a broad range of buffers and in biological media, coupled with compatibility with easy to implement conjugation techniques. This allows the immobilization of specific biomolecules (e.g., peptides and proteins) on the nanocrystal surfaces to form functional platforms that can be used for developing NP-based sensing, imaging, and in vivo tracking.

It has already been well-established that (for cap exchange) stability of the nanocrystals is determined by the nature of the capping ligand and its affinity to the inorganic nanocrystal surface. Anchoring groups, such as thiols, histidines, and amines, have been used for ligand exchange.[10,40−42,44−46] The overall mechanism for interaction and binding to the nanocrystals is driven by coordination chemistry (i.e., dative not covalent binding). Among these, thiol groups exhibit stronger affinity to several metal and semiconductor surfaces. Thiol-appended ligands have been used by several groups to cap ZnS-overcoated nanocrystals (CdSe–ZnS and others).[39−42,47−49]

We have reported in an early study that CdSe–ZnS QDs capped with dihydrolipoic acid (DHLA) exhibit much better stability than those cap-exchanged with monothiol appended ligands (due to the chelating effect of the bidentate anchoring group), even though long-term stability was limited to basic buffer conditions.[39] Subsequently, we and other groups have developed poly(ethylene glycol) (PEG)- and zwitterion-appended DHLA ligands and shown that QDs cap-exchanged with these materials exhibit enhanced stability over a broad range of biological conditions, such as high electrolyte concentration, and over a wide range of pHs.[40-42,48,50] In a more recent report, we have used the Michael addition to append two thioctic acid (TA) or DHLA (after reduction of the dithiolane ring) groups onto the PEG, producing a higher coordination onto AuNP and QD surfaces, respectively.[47] The bis(TA)–PEG and bis(DHLA)–PEG ligands substantially improved the stability of water dispersions of AuNPs and QDs compared to monothiol- and dithiol-terminated analogues. Nonetheless, we found that further functionalization of those ligands with reactive groups was tedious. These findings clearly indicate that increased coordination of the ligand onto the nanocrystal surface provides clear benefits. Other authors focused on increasing the coordination to the metal surfaces by grafting a few mercaptoethylamine groups onto a short poly(acrylic acid) (PAA) backbone; ∼15% of the carboxy

dx.doi.org/10.1021/la203968t | *Langmuir* 2012, 28, 2761−2772

groups were reacted with mercaptoethylamine groups. These polymer ligands allowed the transfer of QDs to water media.[51] Dispersion in water relied on the availability of several carboxy groups on the nanocrystals. Using similar concepts, Raymo and co-workers designed a capping polymer construct made of polymethacrylate chain appended with several lateral PEG2000 chains, some of them end-functionalized, and a few TA anchoring groups and applied these polymers to transfer CdSe–ZnS QDs to buffer media.[52,53]

Building on those rationales and using a simple synthetic design, we developed a new set of OligoPEG ligands that combine increased coordination to metal and semiconducting nanocrystal surfaces, affinity to aqueous media, and chemical reactivity. For this we have used low molecular weight poly(acrylic acid) ($M_W \sim 1800$, $N_w \sim 25$) as a central backbone onto which we grafted laterally and simultaneously several copies of TA–PEG and methoxy-PEG moieties. The TA–PEG and H_3CO–PEG grafting on the poly(acrylic acid) (to provide OligoPEG–TA) used a simple approach based on DCC coupling. As prepared the OligoPEG–TA can be used for capping AuNPs, while reduction of the TA (to DHLA) provides OligoPEG–DHLA ligands, which can be used for capping ZnS-overcoated QDs. Our design further allowed incorporation of specific functionalities such as azides and amines within the ligand structure. Overall, the OligoPEG ligands exhibit a few unique features: (i) multiple TA or DHLA anchoring groups grafted on a single PAA oligomer, (ii) multiple PEG segments, and (iii) a tunable number of reactive groups (functionalities). We found that cap exchange with these ligands provided QDs and AuNPs that exhibit remarkable stability to pH changes and to added excess of electrolyte and are compatible with simple conjugation strategies to biomolecules. We also found that much smaller amounts of excess ligands than those used for DHLA–PEG, for example, were required, while cap exchange of QDs could be carried out at room temperature.

EXPERIMENTAL SECTION

Materials. All syntheses described in this study were carried out under N_2 passed through an O_2 scrubbing tower unless otherwise stated. Standard Schlenk techniques were used when manipulating air-sensitive reactions, while air-sensitive materials were handled in an MBraun Labmaster 130 glovebox (Stratham, NH). Poly(acrylic acid) (molecular weight average ~1800), poly(ethylene glycol) (molecular weight average of 600 and 750), triphenylphosphine, thioctic acid, DMAP (4-(*N*,*N*-dimethylamino)pyridine), DCC (*N*,*N*-dicylohexylcarbodiimide), triethylamine, sodium borohydride, methanesulfonyl chloride, organic solvents (DMF, $CHCl_3$, etc.), PBS buffer, and salts (such as NaCl, Na_2SO_4, Mg_2SO_4) were purchased from Sigma Chemicals (St. Louis, MO). Sodium azide was purchased from Alfa Aesar (Ward Hill, MA). The chemicals and solvents were used as purchased unless otherwise specified. Deuterated solvents were purchased from Cambridge Isotope Laboratories (Andover, MA) and used as received. Column purification chromatography was performed using silica gel (60 Å, 230–400 mesh, from Bodman Industries, Aston, PA). Monoreactive *N*-hydroxysulfosuccinimide (sulfo-NHS)–Cy3 dye and PD10 column were purchased from GE Healthcare (Piscataway, NJ), whereas the peptide was acquired from Peptide International (Louisville, KY). The molar amounts of the PEG derivatives were calculated using the average molecular weight of the corresponding PEG (e.g., PEG ~600 or 750).

Instrumentation. ^{1}H NMR spectra of all compounds were recorded using 600 MHz spectrometer (Bruker SpectroSpin 600 MHz). Fourier transform infrared (FT-IR) spectra of the final purified compounds were measured from Perkin-Elmer FT-IR spectrometer. Optical absorption measurements were carried out using a Shimadzu UV–vis absorption spectrophotometer (UV 2450 model), whereas the fluorescence spectra were collected on Fluorolog-3 spectrometer (Jobin Yvon Inc., Edison, NJ) equipped with PMT and CCD detectors. Solvent evaporation was carried using a lab-scale Buchi rotary evaporator R-215 (New Castle, DE).

Synthesis and Design: PEG Modification of Poly(acrylic acid). The OligoPEG ligands we developed for the stabilization of metallic and semiconductor nanoparticles were synthesized by laterally grafting on a commercially available short-chain PAA one or a combination of TA–PEG600–NH_2, H_3CO–PEG750–NH_2 and N_3–PEG600–NH_2 moieties; these molecular-scale ligands were designed and prepared in our laboratory using synthetic schemes we have described in previous reports.[40,42] Grafting of aminated-PEG moieties (**1**, **2**, and/or **3** shown in Figure 1) onto the PAA backbone relied on DCC-mediated reaction between amine and carboxy groups, in the presence of a catalytic amount of DMAP; the list of prepared compounds is provided in Table 1. The grafted PEG moieties present a combination of anchoring groups for tight binding to the nanocrystal surfaces and a mixture of azide and methoxy terminal groups; the methoxy groups are used to control the fraction of reactive groups, which can be used for further modification and coupling to target molecules. The preparation of diazide-functionalized PEG600 is detailed in the Supporting Information.

Table 1. List of OligoPEG Ligands Prepared in This Study[a]

OligoPEG compd(s)	fraction of OCH_3–PEG moieties (as %)	fraction of TA–PEG moieties (as %)	fraction of N_3–PEG moieties (as %)
4A	~64–68	~28	
4B	~44–48	~44–48	
6A	~40–44	~44–48	~4–8
6B	~32–36	~44–48	~8–12
6C	~40–44	~36–40	~8–12

[a]Also provided are relative fractions of the various PEGylated moieties grafted along the PAA backbone.

Methoxy OligoPEG–TA, 4A and 4B. Compounds **4A** and **4B** have similar structure, except that **4A** has a slightly lower grafting fraction of TA–PEG moieties; for **4A** we used a nominal ratio of TA–PEG–NH_2 to COOH (on the PAA) of ~30%, whereas for **4B** that ratio was increased to ~50%; we detail the synthesis of **4B**. Poly(acrylic acid) (1.0 g, ~0.56 mmol) and 50 mL of dimethylformamide (DMF) were placed in a 250 mL round-bottom flask, and the mixture was cooled to ~0 °C. DCC (2.9 g, 14.0 mmol) was added under ice-cold conditions, and the mixture was stirred for ~30 min, followed by heating to ~85 °C. When the temperature of the mixture is equilibrated, a solution containing TA–PEG600–NH_2 (5.5 g, 7.0 mmol) and H_2N–PEG750–OCH_3 (5.3 g, 7.0 mmol) in DMF (30 mL) was added slowly, followed by DMAP (225 mg, 1.9 mmol), and the reaction mixture was left stirring for 4 days under nitrogen atmosphere before removing the dicyclo urea (DCU) side-product by filtration. DMF was removed under vacuum, then 100 mL of distilled water was added to the residue, and this mixture was washed with diethyl ether (100 mL, two times) to remove residual DCU, followed by washing with ethyl acetate (100 mL, two times).[54] The mixture was lyophilized to remove the water, and the crude product was dissolved in $CHCl_3$. The solution containing the crude product was filtered to remove unreacted PAA, slightly dried, and then chromatographed on a silica column (230–400 mesh) using a mixture of chloroform–methanol (20:1) as the eluent; this procedure yielded the compound **4B** as a viscous dark-yellow liquid (7.0 g, ~65% yield).

^{1}H NMR (600 MHz, $CDCl_3$) for compound **4A**: δ 6.41 (br, s), 3.77–3.57 (m), 3.58–3.54 (m, 96H), 3.48–3.40 (m, 22H), 3.37 (s, 49.82H), 3.2–3.14 (m), 3.13–3.07 (m), 2.48–2.40 (m, 8H), 2.41–2.22 (br, 25H), 2.18 (t, J = 7.8 Hz, 14H), 1.93–1.85 (m), 1.84–1.73 (br), 1.72–1.04(m). IR (neat): 3327.5, 2870, 1655.6, 1544.4, 1348.5, 1289.2, 1250.4, 1097.9, 948 cm^{-1}.

dx.doi.org/10.1021/la203968t | *Langmuir* 2012, 28, 2761–2772

^{1}H NMR (600 MHz, $CDCl_3$) for compound **4B**: δ 6.36 (br s), 3.77−3.56 (m), 3.55−3.52 (m, 46H), 3.48−3.42 (m, 15H), 3.36 (s, 34.95H), 3.2−3.16 (m), 3.12−3.07 (m), 2.48−2.40 (m, 8H), 2.41−2.22 (br, 25H), 2.18 (t, J = 7.2 Hz, 22.22H), 1.91−1.87 (m), 1.86−1.75 (br), 1.74−1.01(m). IR (neat): 3335.8, 2866.6, 1652, 1540.2, 1452.6, 1348.9, 1290.5, 1251.6, 1094.6, 947 cm^{-1}.

Azide-Functionalized OligoPEG−TA, 6A, 6B, and 6C. To synthesize compound **6A**, poly(acrylic acid) (1.0 g, ∼0.56 mmol) and DCC (2.9 g, 14.0 mmol) were dissolved in DMF (50 mL) in a 250 mL round-bottom flask and stirred for 30 min under ice-cold conditions. A solution of DMF (30 mL) containing TA−PEG600−NH_2 (5.5 g, 7.0 mmol), N_3−PEG600−NH_2 (0.45 g, 0.7 mmol), and H_2N−PEG750−OCH_3 (4.72 g, 6.3 mmol) was added to the flask, and the reaction mixture was heated to ∼85 °C followed by the addition of DMAP (225 mg, 1.9 mmol). After 4 days of stirring at ∼85 °C, DCU was removed by filtration and DMF was removed under vacuum. Then 50 mL of distilled water was added to the residue, and the aqueous layer was first washed with diethyl ether (100 mL, one time), then with ethyl acetate (100 mL, two times). The solution was lyophilized, and the residue was redissolved in chloroform and filtered to remove the precipitate if any. The solvent was evaporated, and the residue was chromatographed on silica gel using chloroform−methanol (15:1) mixture as the eluent, to isolate compound **6A** (6.5 g, yield ∼62%) as a yellow gel; in compound **6A** we anticipate that ∼5% of the total monomer units are grafted with azide-PEG.

Using this reaction route it is possible to vary the relative fraction of the PEG moieties inserted along the PAA backbone. For instance, we prepared two additional compounds **6B** and **6C** where either the relative fractions of azide to methoxy groups or methoxy to TA were varied (see Table 1). For **6B** we used N_3−PEG600−NH_2 (0.87 g, 1.4 mmol), H_2N−PEG750−OCH_3 (4.2 g, 5.6 mmol) while maintaining the amount of TA−PEG600−NH_2 (5.5 g, 7.0 mmol); this is expected to provide a ligand that has ∼10% of the total grafted PEG moieties presenting terminal azides. For **6C** a different stoichiometry oligomer is expected, with TA−PEG (∼36−40%) and PEG−OCH_3 (∼40−44%) while PEG−N_3 is ∼10% (see the Supporting Information for more details).

^{1}H NMR (600 MHz, $CDCl_3$) of compound **6A**: δ 6.22 (br s), 3.76−3.56 (m), 3.54−3.52 (m, 67H), 3.44−3.41 (m, 26H), 3.39−3.37 (t, J = 2.8 Hz, 2.6H), 3.36 (s, 30.94H), 3.18−3.14 (m), 3.12−3.07 (m), 2.48−2.42 (m, 11.9H), 2.41−2.22 (br, 25H), 2.18 (t, J = 7.6 Hz, 22.21H), 1.92−1.86 (m), 1.8−1.73 (br), 1.73−1.04(m). IR (neat): 3330.3, 3008.6, 2872.7, 2107.3, 1663.6, 1544.4, 1452.8, 1350.2, 1293.5, 1452.8, 1350.2, 1293.5, 1250.4, 1092.3, 950.9 cm^{-1}.

Methoxy-OligoPEG−DHLA, 5B: Reduction of the Dithiolane Rings. A solution of compound **4B** (3.5 g, ∼0.18 mmol) dispersed in methanol−water mixture (2:1, v/v, 24 mL) was cooled in an ice-bath, and $NaBH_4$ (760 mg, ∼2.0 mmol) dissolved in water (2 mL) was added dropwise with vigorous stirring. The reaction mixture was then left stirring for 10 h at room temperature. A solution of 1 N hydrochloric acid was added dropwise until the pH of the solution reached ∼6−7. Methanol was evaporated under vacuum, and the aqueous layer was lyophilized to remove water. Chloroform was added to dissolve the compound followed by removal of salts by filtration. The solution was dried over Na_2SO_4, filtered, and solvent was evaporated to obtain the product **5B** as a colorless viscous liquid (2.0 g, yield ∼58%). A similar procedure was used to prepare **5A** by reduction of **4A**.

^{1}H NMR of compound **5A** (600 MHz, $CDCl_3$): δ 6.4 (br s), 3.73−3.60 (m), 3.59−3.55 (m, 77H), 3.49−3.44 (m, 18H), 3.37 (s, 46H), 2.97−2.91 (m), 2.78−2.65 (m), 2.37−2.24 (br, 25H), 2.21 (t, J = 7.2 Hz, 15H), 1.96−1.89 (m), 1.80−1.49 (m), 1.49−1.30 (m), 1.27−1.24(m). IR (neat): 3319.8, 2870, 1655.3, 1649.9, 1538.2, 1455.7, 1360, 1335.9, 1222, 1048, 933.6 cm^{-1}.

^{1}H NMR of compound **5B** (600 MHz, $CDCl_3$): δ 6.35 (br s), 3.74−3.60 (m), 3.57−3.51 (m, 77H), 3.51−3.46 (t, J = 5.5 Hz, 12H), 3.47−3.42 (m, 22H), 3.38 (s, 34.54H), 2.95−2.89 (m), 2.77−2.64 (m), 2.62−2.47 (br, 25H), 2.19 (t, J = 8.0 Hz, 21.81H), 1.97−1.30 (m), 1.26−1.20(m). IR (neat): 3323.8, 2866.6, 1648, 1646.7, 1452.6, 1348.9, 1297, 1248.3, 1096, 947.5 cm^{-1}.

Amine-OligoPEG−DHLA, 7A. A solution of compound **6A** (3.4 g, ∼0.17 mmol) in methanol−water (2:1, v/v, 24 mL) was cooled in an ice-bath, and $NaBH_4$ (850 mg, ∼2.3 mmol) dissolved in water (2 mL) was added dropwise under N_2 atmosphere with stirring. Once addition is complete, the reaction mixture was allowed to stir for 10 h at ambient temperature, and 1 N hydrochloric acid was added dropwise until the pH of the solution reached ∼6.5. Methanol was evaporated under vacuum at ∼35−40 °C, and then the aqueous layer was lyophilized to remove water. The compound was dissolved in chloroform, and residual salts were removed by filtration. The organic solution was dried over Na_2SO_4, filtered, and evaporated to obtain the product as colorless viscous liquid at room temperature (2.1 g, yield ∼62%).

^{1}H NMR (600 MHz, $CDCl_3$): δ 6.3 (br, s), 3.74−3.56 (m), 3.57−3.52 (m, 71.2H), 3.46−3.41 (m, 25.1H), 3.36 (s, 30.9H), 3.19 (br), 2.94−2.89 (m), 2.77−2.63 (m), 2.63−2.48 (br, 25H), 2.18 (t, J = 7.6 Hz, 21.75H), 1.97−1.3 (m), 1.23(m). IR (neat): 3323.8, 2866.6, 1650, 1546.7, 1455.9, 1348.5, 1300.2, 1245, 1092.8, 950 cm^{-1}.

Reduction of compound **6B** (to provide **7B**) followed the same procedure described above for **6A**, starting with 3.38 g of OligoPEG−TA (**6B**), though a slightly higher amount of $NaBH_4$ (900 mg, ∼2.4 mmol) was used. The procedure yielded product **7B** as a colorless liquid at room temperature (1.9 g, yield ∼50%). ^{1}H NMR peak location and assignments are identical to the above (**7B**). IR (neat): 3328, 2868, 1662.8, 1543.6, 1455, 1386.2, 1349.6, 1291.5, 1248, 1094.7, 947.8 cm^{-1}.

Quantum Dots and Gold Nanoparticles. We used three sets of luminescent CdSe−ZnS QDs with maximum emission centered at 543 nm (green), 575 nm (yellow), and 617 nm (red). All QD samples were synthesized using a stepwise reaction based on reducing organometallic precursors at high temperature in a coordinating solvent mixture; further details were reported in previous references.[2,20,21,55,56] Citrate-stabilized Au nanoparticles of sizes 10 and 15 nm diameter were purchased from Ted Pella, (Reading, CA) and used for cap exchange with the various OligoPEG ligands.

RESULTS AND DISCUSSION

Synthesis and Characterization of Multifunctional Ligands. The present design is motivated by previous observations, which have cumulatively shown that the presence of multiple coordinating groups in the ligands promotes stronger anchoring to the inorganic surfaces of QDs and AuNPs and provides improved colloidal stability to the nanocrystals following cap exchange.[39−41,47,48] In addition, the insertion of PEG moieties within the ligand structure provides water and biological compatibility while reducing nonspecific interactions.[35,41,57−60]

As an alternative approach we have reasoned that starting from a short PAA chain we can combine multiple coordinating and reacting groups in the same structure using our developed NH_2−PEG moieties to prepare a new set of multifunctional PEGylated oligomers (OligoPEG). These oligomers present three sets of PEG moieties: one set is appended with TA (or DHLA) for strong anchoring onto the nanocrystals, another set presents terminal reactive groups such as azide and amine, whereas the third has terminally inert groups (methoxy here). The methoxy-terminated PEG moieties provide the means of controlling the fraction of TA−PEG anchoring and reactive N_3/NH_2−PEGs along the oligomer and on the final nanoparticle after transfer to buffer media.

Figure 1 shows a schematic representation of the synthetic procedure, the steps involved, and the structure of the multifunctional oligomers prepared. Our scheme used a series of PEG moieties with the desired chain length and functional/reactive groups. TA−PEG−NH_2, N_3−PEG−NH_2 (PEG M_w ∼ 600), and H_3CO−PEG−NH_2 (M_w of PEG ∼750) were first

dx.doi.org/10.1021/la203968t | Langmuir 2012, 28, 2761−2772

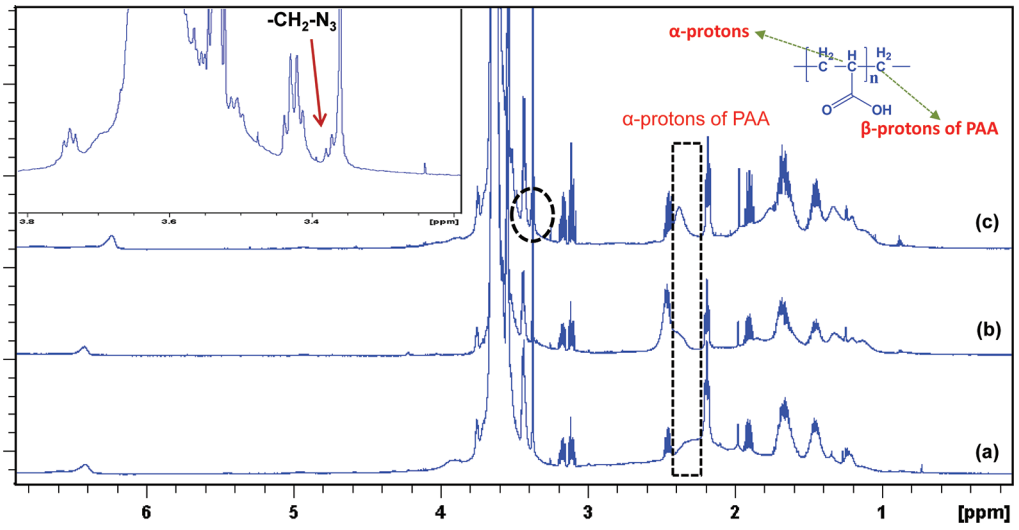

Figure 2. ^{1}H NMR spectra of OligoPEG ligands in $CDCl_3$: (a) compound **4A**, (b) compound **4B**, (c) compound **6A**. Inset: expansion of spectrum of compound **6A** showing the small peak ascribed to N_3 near 3.36 ppm. Integration: compound **4A** (δ 3.36, s, 49.82H; δ 2.41−2.22, br, 25H; δ 2.18, t, 14 H), compound **4B** (δ 3.36, s, 34.95H; δ 2.41−2.22, br, 25H; δ 2.18, t, 22.22H), compound **6A** (δ 3.36, s, 30.94H; δ 2.41−2.22, br, 25H; δ 2.18, t, 22.21H).

prepared according to our previous method.[40,42,57] The OligoPEG ligand synthesis used DCC condensation to react amines on the PEG moieties with carboxylic acids on the PAA. This allowed the simultaneous incorporation of anchoring, hydrophilic, and reactive groups/moieties into the same oligomer structure. Proper balance between the TAs and PEG moieties is essential to render the nanocrystals cap-exchanged with these ligands dispersible in buffer media. Here oligomers with ∼7−12 TA−PEG moieties (or 28−48% of the total monomer units on the PAA) were prepared and tested. The as-prepared TA-modified OligoPEG ligands interact with AuNPs, while subsequent reduction of the dithiolane rings in the presence of sodium borohydride ($NaBH_4$) provides OligoPEG−DHLA, which can be used to transfer TOP/TOPO-capped QDs to buffer media. Furthermore, this strategy allowed us to introduce N_3 or NH_2 (obtained via reduction of N_3) functionalities in the final ligands; these can be used for orthogonal coupling to biological molecules.

Remark. We should note that balance between the number of TAs and PEGylated moieties grafted along the PAA backbone is important. For instance, we found that grafting a higher fraction of TA−PEG moieties (e.g., on more than ∼50% of the total monomers) can produce hydrophobic oligomers, presumably attributed to sulfur−sulfur bridging. We found that adding a strong reducing agent such as $NaBH_4$ renders such as materials soluble in water solutions. Here, we focused on OligoPEG containing ∼11−12 or smaller numbers of TA−PEG moieties.

Ligand Characterization. Characterization of the ligands relied on ^{1}H NMR and FT-IR measurements. Figure 2 shows ^{1}H NMR spectra of three representative TA-appended OligoPEG ligands prepared in this study (namely, **4A**, **4B**, and **6A**). Data show that each spectrum combines the individual signatures of the PEG (PEG600, PEG750) chains, the poly(acrylic acid) backbone, and the thioctic acid groups. The PEG chains produce a large peak around 3.8−3.6 ppm, while the sharp peak at ∼3.36 ppm is ascribed to the OCH_3 groups. The CH_2 repeating groups in the TA produce a broad contribution (multiple peaks spanning the range of 3.5−1.4 ppm) that partially overlaps with the β-protons of PAA; contribution from these β-protons appears as a broad peak at 1.9−1.2 ppm, while that from the thioctic acid protons is at 1.89, 1.66, and 1.44 ppm. The broad peak at ∼2.4−2.2 ppm is characteristic of the α-hydrogens ($n \sim 25$) of PAA. This peak is rather important, as it provides the integration (25 protons) used to calculate the number of PEG moieties grafted onto the PAA chain. The approximate number of TA groups per chain (i.e., grafting percentage) was determined on the basis of comparing the peak area obtained from −CH groups (α-hydrogens) of PAA at ∼2.4−2.2 ppm with that from the $-CH_2$ groups of TA at 2.1 ppm (t, 2H). Conversely, the number of methoxy-PEG segments was extracted from the sharp singlet peak at ∼3.36 ppm (ascribed to OCH_3 groups); this peak was used as reference with respect to α-hydrogens of PAA.

Analysis of the integration peaks of the spectra shown in Figure 2 for compounds **4A** and **4B** provided estimates for the percentage of the overall grafting along the PAA backbone: we measured the following ligand stoichiometry: **4A**, TA−PEG (∼28% or ∼7.0 TAs), PEG−OCH_3 (∼64−68% or ∼16−17 OCH_3 groups); **4B** TA−PEG (44−48% or ∼11−12 TAs), PEG−OCH_3 (at 44−48% or ∼11−12 OCH_3 groups). For **6A** we measured ∼11−12 TA−PEG (44−48%) and 10−11 H_3CO−PEG (∼40−44%) and ∼1−2 (∼4−8%) azides, whereas for and **6B** we estimated ∼11−12 TA−PEG (44−48%) and 8−9 PEG−OCH_3 (∼32−36%) and 2−3 (∼8−12%) azides; the azide fractions were calculated using the integration for the small shoulder peak at 3.4 ppm, next to the methoxy peak at 3.36 ppm (see Figure 2).

Overall, the ^{1}H NMR data provide a good and fairly accurate account for the composition of the ligands we prepared, with estimates of the relative fractions of the different end-functionalized PEG moieties grafted along the PAA backbone. For instance, compounds **6A** and **6B** were prepared starting with the exact same molar amounts of TA−PEG, and the measured numbers of grafted TA groups were essentially identical. Nonetheless, such analysis also indicates that slightly lower than the optimal (100%) coupling to the carboxyl groups on the PAA took place, which may be attributed to the nature of the DCC reaction used; ∼2 COOH groups were left unreacted in the final OligoPEG. FT-IR data also confirmed

dx.doi.org/10.1021/la203968t | *Langmuir* 2012, 28, 2761−2772

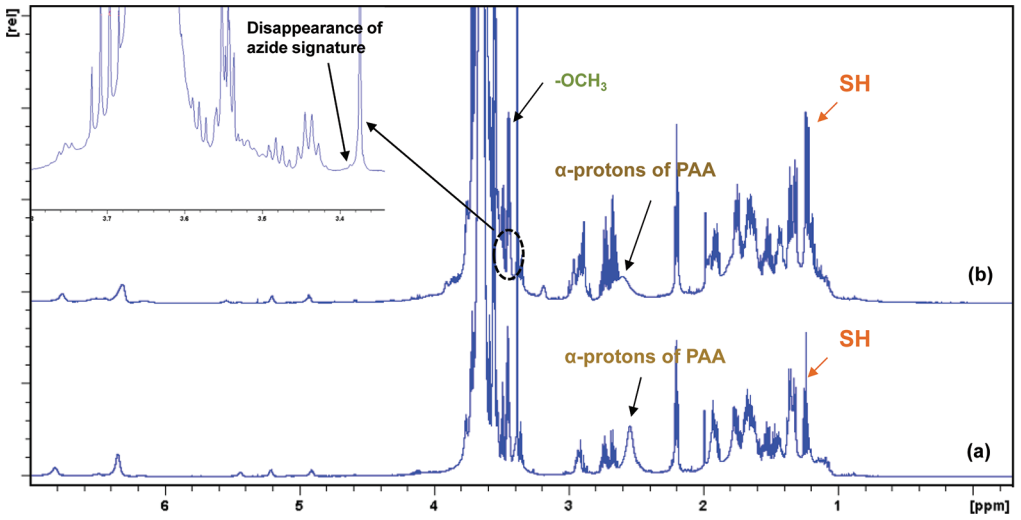

Figure 3. ^{1}H NMR spectra of reduced OligoPEG ligands in $CDCl_3$: (a) compound **5B**, (b) compound **7A**. The inset shows an expansion of the spectrum around 3.3−3.7 ppm; the peak due to CH_2 attached to the N_3 group has indeed vanished after borohydride reduction.

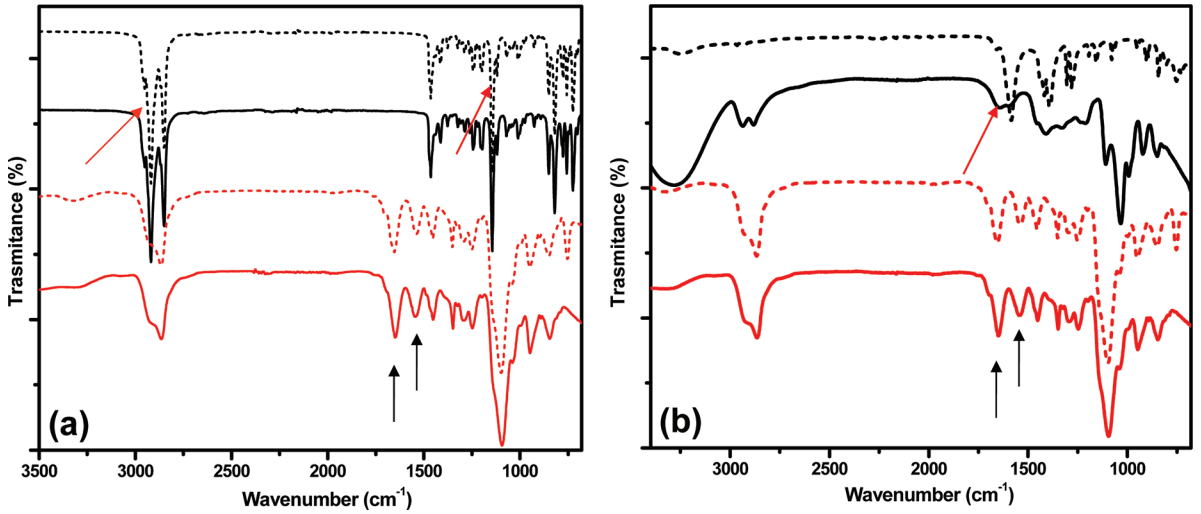

Figure 4. FT-IR spectra of (a) TOPO ligand only (black, broken line), TOP/TOPO-capped QDs in toluene (black, solid line), OligoPEG ligand **5B** pure (red, broken line), and OligoPEG-capped QDs in water (red, solid line) after ligand exchange. The top arrows refer to the peaks ascribed to CH stretching (at ∼2917, 2849 cm^{-1}) and P═O stretching (at ∼1144 cm^{-1}) of TOPO, whereas the bottom arrows designate the new peaks ascribed to the amide band of the OligoPEG (at ∼1648 and ∼1546 cm^{-1}). (b) Tribasic citrate ligand only (black, broken line), citrate-stabilized AuNPs (black, solid line), OligoPEG ligand **4B** pure (red, broken line), and OligoPEG-capped AuNPs in water (red, solid line). The top arrow designates the COOH band of the citrate, whereas the bottom ones designate the amide bands as provided in panel (a).

that a small fraction of the carboxyl groups stayed intact (see the Supporting Information).

Figure 3 shows two representative ^{1}H NMR spectra of compounds **5B** and **7A**, obtained after the borohydride reduction of **4B** and **6A**, respectively. The peaks at ∼3.1 and 2.4 ppm shifted to ∼2.8 and 2.7 ppm, respectively, while a new triplet peak characteristic of the −SH protons appeared at ∼1.2−1.3 ppm. This clearly indicates that the borohydride reduction of the TA groups was unaffected by coupling onto the PAA and it did not alter the structure of OligoPEG ligands. Nonetheless, we found that the peak at ∼3.4 ppm (indicative of azide signature) disappeared; this indicates that a transformation of the azide groups to amines has taken place, as is often the case for free TA−PEG−N_3 molecules in presence of $NaBH_4$. FT-IR data confirm this transformation, as the peak at ∼2100 cm^{-1} disappeared from the spectrum after borohydride reduction.

We should emphasize that the present design presents a clear advantage as one can simultaneously vary the number of thiol ligands, to control the binding efficiency, and the number of reactive groups on the OligoPEG according to specific requirements. If combined with modification of the nature of the reactive groups, this will allow further flexibility and control over the biological coupling and targeting of the nanocrystals.

Cap Exchange and Nanoparticle Functionality. Ligand exchange of both gold nanoparticles and QDs was performed using our new OligoPEG ligands. The OligoPEG−TA ligands can be used to cap AuNPs. However, borohydride ($NaBH_4$) reduction of the 1, 2-dithiolane groups (to DHLAs) was necessary for performing ligand exchange with CdSe−ZnS QDs. We used two sets of citrate-stabilized AuNPs having 10 and 15 nm diameters, and three samples of TOP/TOPO-capped QDs emitting at $\lambda_{em} \cong$ 543, 575, and 617 nm. We found that cap exchange of AuNPs with OligoPEG−TA and QDs

dx.doi.org/10.1021/la203968t | *Langmuir* 2012, 28, 2761−2772

with OligoPEG−DHLA could be carried out using smaller amounts of ligands than what is routinely used with their molecular counterparts (TA/DHLA−PEG series).[40,57] Essentially, the amount of OligoPEG ligands needed for cap exchange was about one-half of that of TA− or DHLA−PEG ligands. Similarly, we found that cap exchange of QDs could be performed at lower (even room) temperature. For a typical QD cap exchange, 3 mL of growth solution (~9.0 μM) in a mixture of hexane and toluene was first precipitated using ethanol, centrifuged, and the supernatant discarded yielding a wet pellet of QDs. To this pellet OligoPEG−DHLA (**5B**, ~700 mg) or DHLA−PEG (~1.5 g) ligands dissolved in 0.5−1 mL of ethanol was added along with a few drops (5−6) of 1 M tetramethyl ammonium hydroxide (TMAH) solution in ethanol. The mixture was then heated at 40−45 °C for several hours under nitrogen atmosphere with stirring, followed by precipitation of QDs using chloroform and hexane mixture. Following removal of the solvents the QDs were dispersed in DI water, and excess solubilized free ligands were removed by applying a few rounds of concentration dilution using a membrane filtration device Amicon Ultra 50K (from Millipore). The ligand exchange on the QD was confirmed using FT-IR spectra (see Figure 4). Spectra show that the bands characteristic of TOP/TOPO have disappeared following cap exchange, while new bands at ~1648 cm^{-1} (ascribed to amide I, C═O stretching) and at ~1546.7 cm^{-1} (ascribed to amide II, N−H bending) were measured. Moreover, the spectrum of the OligoPEG-capped QDs is identical to that collected from the pure ligand.

The absorption and emission spectra of the QDs (Figure 5) were essentially unaffected by the transfer to buffer media as

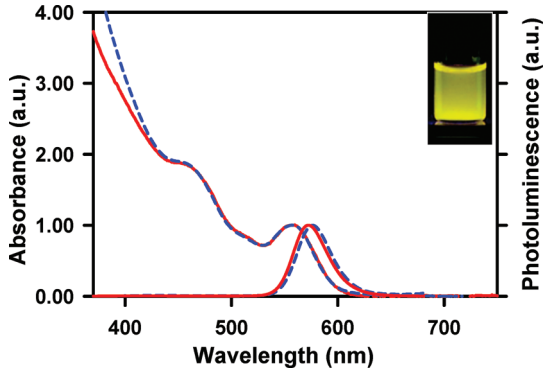

Figure 5. Absorption and fluorescence spectra of QDs ($\lambda_{em} \cong 575$ nm) in toluene (solid line) and in water (broken line) after ligand exchange with OligoPEG ligand **5B**; $\lambda_{ex} = 350$ nm. The inset shows the fluorescence image of a yellow-emitting QD dispersion capped with OligoPEG−DHLA (**5B**) in phosphate-buffered saline (PBS) at neutral pH. The UV−vis and PL spectra were normalized with respect to the band edge peak and maximum emission, respectively.

shown for dispersions of TOP/TOPO-capped (in toluene) and OligoPEG-capped QDs (in DI water). This implies that cap exchange with the new OligoPEG does not alter any of the optical and spectroscopic properties of the nanocrystals, as was reported with DHLA−PEG ligands. Transfer to aqueous media was nonetheless accompanied by a loss in photoluminescence (PL) yield (~25−50% decrease in PL signal) compared to the native TOP/TOPO-capped QDs in toluene. This reduction has been commonly reported for QDs cap-exchanged with thiol-appended ligands including DHLA−PEG series.[40,41,58,61,62]

Cap exchange of citrate-stabilized AuNPs could be carried out using both sets of oligomers, TA- and DHLA-appended, similar to what was reported with the molecular-scale PEGylated ligands.[63] In a typical cap exchange, the required amount of OligoPEG−TA (**4B**, 110 mg) was diluted in 1 mL of DI water and the solution was adjusted to pH 10 by adding a drop of 0.5 M NaOH. This solution was added to citrate-stabilized AuNPs (4 mL, ~1.4×10^{12} particles/mL), and the dispersion was stirred overnight (~18 h) at room temperature.[63] The mixture was then filtered through a 0.45 μm hydrophilic membrane, and excess ligand was removed by washing 2−3 times with DI water using a centrifugal filtration device (Millipore, M_W cutoff of 50 kDa), as described above. Cap exchange of the AuNPs with OligoPEGs (e.g., **4B** and **5B**) was characterized by FT-IR and absorption spectroscopy. FT-IR data collected from AuNP dispersions after cap exchange showed the presence of the amide I band (~1652 cm^{-1}) and amide II band (~1540.2 cm^{-1}); similar to QDs the characteristic features of the ligands remained intact after coordinating with the Au surfaces. We also measured no change in the UV−vis absorption spectra of AuNPs after ligand exchange (see the Supporting Information for further details). We should note that there is a small contribution to the UV−vis absorption spectrum (for $\lambda < 400$ nm) of the hydrophilic OligoPEG−QDs due to the PAA.

Colloidal Stability of OligoPEG-Capped QDs and AuNPs. We tested the stability of aqueous dispersions of OligoPEG-capped nanocrystals over a broad pH range and in the presence of a large excess of NaCl. In previous reports, we have shown that ligand exchange of QDs with DHLA−PEG moieties can provide long-term colloidal stability in buffer solutions over the pH range from 4 to 11.[40,57] A slightly broader pH window (3−12) was achieved using those PEGylated ligands with gold nanoparticles.[57] Therefore, in this study we have focused on the stability of nanocrystals in phosphate buffer media under extreme conditions (pH 2 and pH 14) and in presence of large excess electrolytes (2 M NaCl). Phosphate buffers at pH 2−12 were prepared following standard procedures using different molar ratio of NaH_2PO_4, Na_2HPO_4, Na_3PO_4, or H_3PO_4. Buffers at extreme pH, such as pH 1, pH 13, and pH 14, were prepared by adding a few drops of either HCl or NaOH. All of the buffer solutions contained 0.137 mM NaCl. Aliquots of stock solutions of OligoPEG-capped NPs (~6 μM) were added to the desired buffer to a final concentration of 1 μM and 3 nM for QDs and AuNPs, respectively. Dispersions of DHLA−PEG−OCH_3- or TA−PEG−OCH_3-stabilized nanocrystals at several pHs (at similar concentrations) were used as control. Green-, yellow-, and red-emitting OligoPEG-stabilized QDs and AuNPs were used for the pH stability test.

Figure 6a shows the fluorescence images of a set of yellow-emitting QDs capped with OligoPEG−DHLA (**5B**) at pH values ranging from 2 to 14 in phosphate buffer solutions, immediately following transfer and after 45 days of storage. Figure 6b shows a side-by-side comparison of the same water-dispersed QDs capped with either **5B** or DHLA−PEG−OCH_3 ligands at three different pHs (2, 7, and 14), and in the presence of 1 and 2 M NaCl. The images indicate that the QD dispersions remained homogeneous and optically clear over the full range of pHs and in the presence of 2 M NaCl. We should emphasize that the long-term colloidal stability of the QD dispersions is also accompanied with little to no change in the fluorescence emission. Overall relative variation in the

dx.doi.org/10.1021/la203968t | Langmuir 2012, 28, 2761−2772

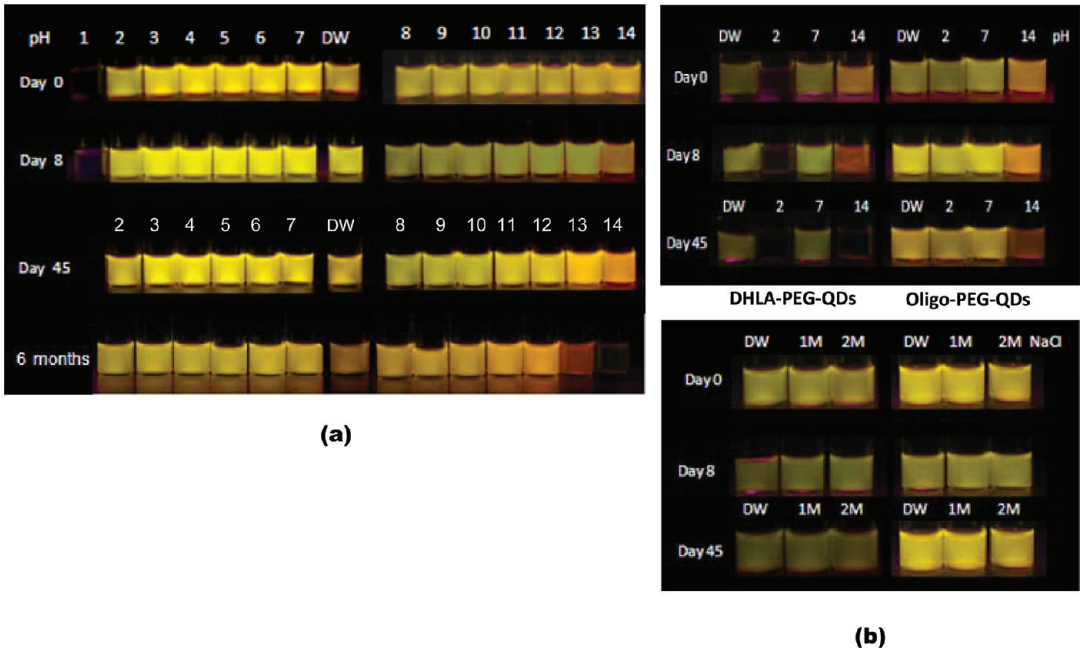

Figure 6. (a) Fluorescence images of CdSe–ZnS QDs ($\lambda_{em} \cong 575$ nm) capped with OligoPEG–DHLA ligand (**5B**) at different pH values and a control sample in deionized water (DW); each vial contains 1 μM QDs in phosphate buffer. No sign of aggregation is observed after 45 days of storage. (b) (top) Fluorescence images of QDs stabilized by both DHLA–PEG–OCH_3 and OligoPEG–DHLA at three different pHs (2, 7, and 14); (bottom) fluorescence images of QDs stabilized by both DHLA–PEG–OCH_3 and OligoPEG–DHLA in the presence of 1 and 2 M NaCl.

fluorescence intensity was small (smaller than 20% after 1 year in the worse case), and it varied from one pH to another. Nonetheless, though the samples at pH 2–13 remained homogeneous and fluorescent for at least 6 months of storage, the dispersion at pH 14 became slightly reddish, and turbidity slowly formed after 3 months, indicative of slow aggregation buildup. In comparison, nanoparticles capped with DHLA–PEG became unstable at pH 2 and 14 after 8 days of storage (Figure 6b). The control dispersions of DHLA–PEG–QDs stayed stable in the presence of excess NaCl, though a slight color change could be seen. Similar long-term stability was observed for QDs dispersed in the growth media (see the Supporting Information).

We also verified that other color QDs cap-exchanged with the OligoPEG ligand **5B** (green emitting with $\lambda_{em} \cong 543$ nm and red emitting with $\lambda_{em} \cong 617$ nm) were also stable and fluorescent over the pH range of 2–13 for at least 3 months (see the Supporting Information). These observations combined clearly indicate that the multithiol-presenting OligoPEG ligands tightly bind onto the QDs surface and promote their long-term stability in a wide range of buffers and in the presence of large excess of electrolytes.

Similar to QDs, AuNPs capped with these OligoPEG–TA ligands exhibited remarkable stability to pH changes and to added NaCl, with no sign of aggregation or changes in the optical absorption spectra for at least 8 months (see Figure 7). We also tested the stability of the AuNPs in the presence of DTT molecules; AuNPs capped with OligoPEG **4A** and **4B** along with NPs capped with TA–PEG–OCH_3 (control) were used. Enhanced NP stability is achieved using OligoPEG ligands **4A** and **4B** compared to control samples. Nonetheless, stability is slightly better for NP capped with **4A**. We suspect that may be due to the larger number of TA groups in OligoPEG **4B** compared to **4A**, which can cause sulfur–sulfur

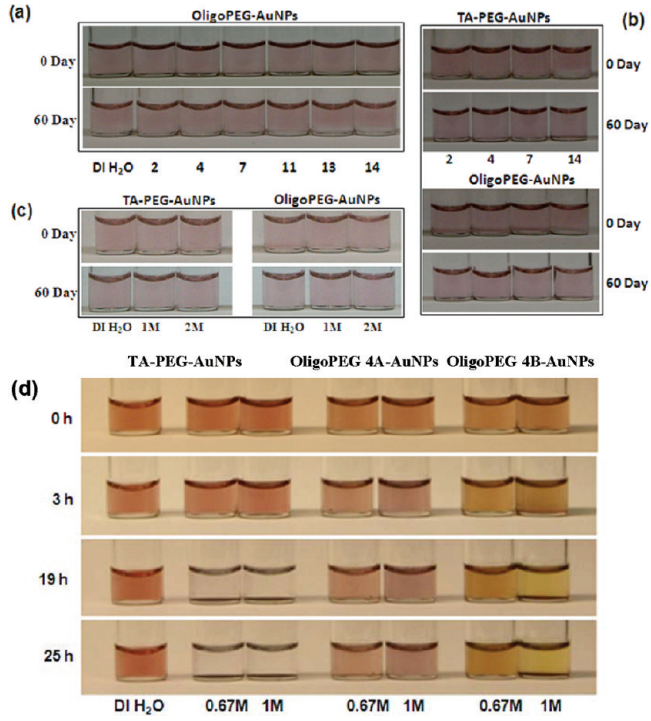

Figure 7. (a) Optical images of AuNPs (10 nm) capped with ligand **4B** (OligoPEG–TA) in phosphate buffer at different pH values; each vial contains 3 nM AuNPs; similar data were collected for the 15 nm AuNPs (see the Supporting Information). (b) Side-by-side optical images of AuNPs stabilized with TA–PEG–OCH_3 and OligoPEG–TA (**4B**) at four pHs (2, 4, 7, and 14). (c) Optical images of AuNPs stabilized with TA–PEG–OCH_3 and **4B** in the presence of 1 and 2 M NaCl. (d) Optical images of AuNPs (10 nm) capped with TA–PEG–OCH_3, **4A** and **4B**, in the presence of 0.67 and 0.1 M DTT and 0. 4 M NaCl; both were tracked over 25 h.

dx.doi.org/10.1021/la203968t | *Langmuir* 2012, 28, 2761–2772

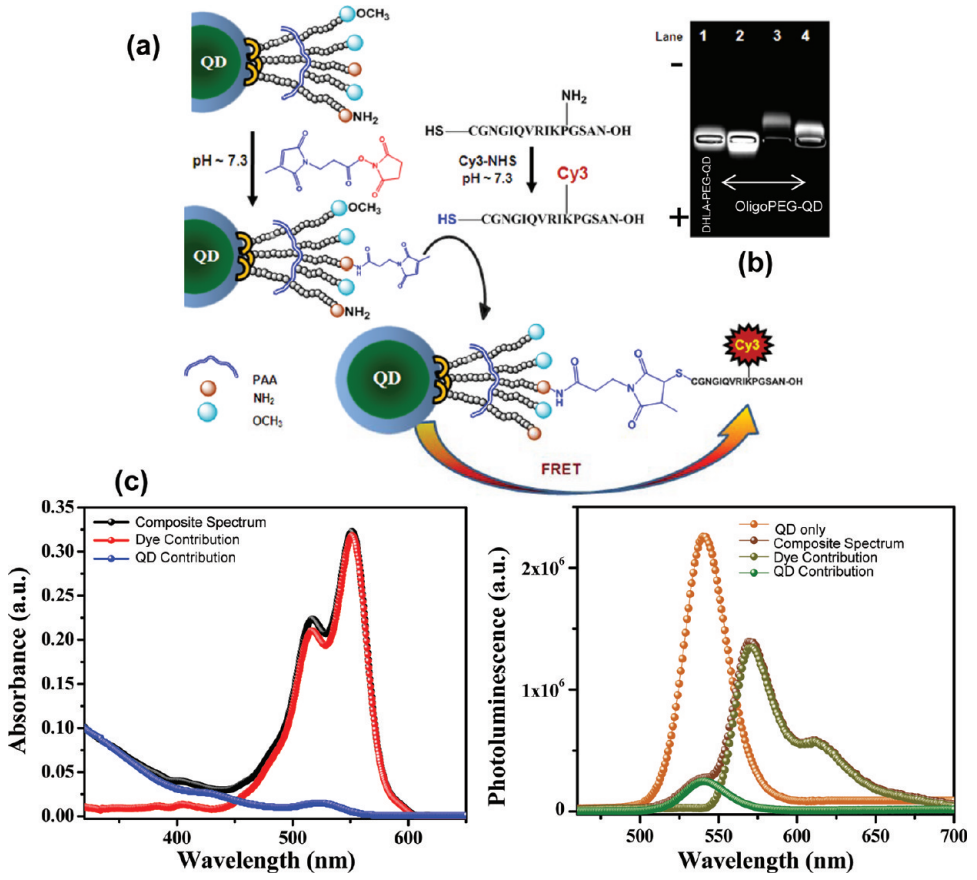

Figure 8. (a) Schematic representation (not to scale) of the coupling strategy used to attach the OligoPEG–DHLA-capped QDs ($\lambda_{em} \cong 543$ nm) with peptide molecules prelabeled with Cy3 dye. (b) Gel eletrophoresis image of QDs capped with OligoPEG ligands: lane 1, QDs capped with DHLA–PEG–OCH_3 (control); lane 2, QDs capped with **5B**; lane 3, QDs capped with **7B** (OligoPEG containing ~10% amines); lane 4, QDs capped with ligand **7A** (OligoPEG containing ~5% amines). (c) (left) UV–vis absorption spectra of QD–peptide–Cy3 conjugate after purification together with the deconvoluted contributions of pure QDs and Cy3 dye. (right) Composite emission spectra of QD–peptide–Cy3 conjugate, together with the deconvoluted contributions from QDs and Cy3 dye. The dispersion was excited at 430 nm, where direct dye excitation is very small.

cross-bridging and potential aggregation in the presence of DTT.

Surface Functionalization of Quantum Dots. The present design also allows easy introduction of functional groups within the ligand structure and the preparation of nanoparticles that present varying numbers of reactive groups on their surfaces. This offers an alternative scheme to those we previously described using molecular-scale DHLA–PEG-based ligands, where end-functionalized and inert ligands were mixed (during cap exchange) in order to achieve surface reactivity.[42] In a preliminary demonstration we used OligoPEG–DHLA ligand presenting a fraction of grafted NH_2–PEG moieties (compound **7A** and **7B**), and tested whether those amine groups were available for further reactions. Figure 8 shows a gel electrophoresis image for four dispersions of green-emitting QDs, three cap-exchanged with OligoPEG **5B**, **7A**, and **7B**, while the fourth was capped with DHLA–PEG–OCH_3 (as control). The QD dispersions were diluted in a 20% glycerol 1× TBE loading buffer (pH 8.5), loaded into 1% agarose gel, then 7.5 V/cm was applied for 30 min; the gel was imaged using Bio-Rad Chemidoc gel imaging system. The image in Figure 8 shows a marginal mobility shift toward the anode for QDs capped with OligoPEG **5B**, whereas no shift was measured for DHLA–PEG–OCH_3-capped QDs (lanes 1 and 2), indicating that the nanocrystals cap-exchanged with **5B** presented a very small negative surface density (i.e., essentially neutral nanocrystals). This is somewhat surprising given the fact that the ^{1}H NMR data indicated that there are one or two uncoupled carboxyl groups along the PAA in the final OligoPEG **5A** and **5B**, and may imply that these groups are completely "shielded" inside the oligomer structure. In contrast, QDs capped with OligoPEG ligands (**7A** and **7B**) designed with a small fraction of aminated PEG moieties (5% and 10% of the total number of PAA monomers) exhibited a mobility shift toward the negative electrode, with slightly larger shift measured for ligands presenting 10% aminated PEG moieties (see lanes 3 and 4 in Figure 8b). This proves that tunable numbers of amines on the nanocrystal are available for further coupling to potential target molecules.

QD–Peptide–Dye Conjugates and Energy Transfer Measurements. We further used a combination of absorption spectroscopy and FRET (fluorescence resonance energy transfer) measurements to extract an estimate for the number of amine groups available on a QD cap-exchanged with compound **7A** (amine-OligoPEG–DHLA). For this 543 nm emitting QDs cap-exchanged with compound **7A** were conjugated to Cy3-labeled peptides as follows (see the schematics in Figure 8): (1) amines on the QDs were transformed to maleimide groups using NHS–methyl maleimide, to make the nanocrystal surface compatible with

dx.doi.org/10.1021/la203968t | *Langmuir* 2012, 28, 2761–2772

cysteine coupling chemistry; (2) NHS−Cy3 was conjugated to the lysine (K) group on a peptide presenting an N-terminal cysteine (CGNGIQVRIKPGSAN); (3) following purification the Cy3−peptide was reacted with maleimide−QDs to yield QD−petide−Cy3 complexes. Additional details about the preparation of the NHS−methyl maleimide, the involved coupling, and purification steps are provided in the Supporting Information.

Figure 8c shows the UV−vis absorption (left) and the photoluminescence (right) spectra collected for a dispersion of QD−peptide−dye conjugates. Both composite spectra show clear contributions from the QD and dye. The absorption spectrum could be deconvoluted to yield the individual contributions of the QDs and Cy3 dye in the sample. From the absorption data and using the available extinction coefficients of both dye (150 000 M^{-1} cm^{-1} at λ = 550 nm) and QDs (7.06×10^5 at λ = 350 nm) we extracted a measure for the molar concentrations of QDs and dye in the dispersion, which we used to deduce an estimate for the average number of Cy3 dyes per QD, $n \sim 22$. Absorption data alone do not necessarily prove coupling of the dye to QDs, however. Analysis of the FRET data, though more complex, is more informative because only close proximity between the QD and dye (due to conjugation) can produce sizable rates of FRET.[64] Figure 8c shows that following coupling between amine−QD and Cy3−peptide, there is a substantial loss in the QD contribution (compared to QD-only control dispersion) coupled with a pronounced enhancement in the dye contribution; direct excitation contribution to the dye emission, subtracted from the composite spectrum, is small as we excite the system far from the dye peak.[65] These observations were further supported by time-resolved fluorescence measurements, where a substantial decrease in the exciton lifetime of the QDs (donor) was measured for the conjugates (see the Supporting Information). Quantitative estimate of the lifetime changes is difficult, nonetheless, due to the sizable spectral overlap between QD and dye emissions. We attribute these results (PL data shown in Figure 8c and time-resolved data shown in the Supporting Information) to nonradiative transfer of excitation energy from the QD (donor) to proximal dyes, as a result of conjugate formation.

The FRET efficiency E is measured experimentally using

$$E = \frac{F_D - F_{DA}}{F_D} \quad (1)$$

where F_D and F_{DA} are the fluorescence intensities collected from the donor alone and donor in the presence of the acceptor(s), respectively. To extract an estimate for the value of n, we use a simplified expression of the FRET efficiency we previously demonstrated for a centrosymmetric system (made of one central donor and n acceptors, all arrayed at a given separation distance, r, from the center of the donor), E_n, expressed as[65]

$$E_n = \frac{nR_0^6}{nR_0^6 + r^6} \quad (2)$$

where the Förster radius, R_0, designates the separation distance (for one-donor−one-acceptor system) corresponding to $E_{n=1}$ = 0.5 and is given by[64]

$$R_0^6 = (9.78 \times 10^3)(n_D^{-4} \kappa_p^2 Q_D I) \quad (3)$$

R_0 (expressed in angstroms) depends on the PL quantum yield of the donor, Q_D, the refractive index of the medium n_D, Avogadro's number, N_A, the dipole orientation parameter, κ_p, and the spectral overlap integral, I.[64] The orientation factor κ_p^2 = 2/3 for our present configuration. I is extracted from integration (over all wavelengths) of the spectral overlap function, $J(\lambda) = PL_{D\text{-}corr}(\lambda)\lambda^4\varepsilon_A$; where PL_D and ε_A designate the normalized fluorescence spectrum of the donor and the extinction coefficient spectrum of the acceptor, respectively.[64] Though most of the parameters in the expression for E_n are extracted from the experimental data, a judicious consideration of the conjugate configuration and estimation of r are important, as they play an important role in extracting a value for n, due to the sixth power dependence of E_n on r. Table 2 shows the values for the various experimental parameters used for the present analysis.

Table 2. Overlap Integral, Quantum Yields, Förster Radius/Distance, and the Estimated Number of Acceptors in the QD−Pep−Cy3 Conjugate

donor−acceptor pair	543 nm QD−Cy3
overlap integral, $I \times 10^{13}$ (cm^3/M)	7.61
quantum yield	0.25
Förster distance, R_0 (Å)	57.3
no. of acceptor(s)	∼20−21

For our system, we use an estimate for the separation distance $r \sim 67$ Å (assuming a QD radius of ∼30 Å, a capping layer of ∼20 Å, a peptide segment between maleimide and dye location of ∼12 Å; we assume that the dye center is located at 5 Å from the linker site). Using this information we estimate that there are ∼21 Cy3 dyes per QD assembly.[65,66] This value is very close to the one estimated from the UV−vis data above. If we assume a complete maleimide transformation of all the amines on the QD and 100% coupling efficiency between the cysteines and maleimides, we anticipate that a green-emitting core−shell QD cap-exchanged with OligoPEG−DHLA (**7A**) presents ∼20 amine reactive sites. This is certainly an underestimated value, as the reactions involved are naturally less than 100% efficient. Nonetheless, the consistency of the estimates extracted from the spectroscopy data implies that the reactive amines in the oligomer structure are available for further modification and coupling to target biomolecules.

CONCLUSION

We have reported a simple and straightforward synthetic strategy to develop a set of multifunctional, multidentate PEGylated oligomer (OligoPEG) ligands with tunable numbers of metal-coordinating thiols and reactive groups. The synthesis scheme relied on DCC/DMAP coupling and allowed grafting of a controllable number of surface-coordinating, or end-reactive, PEGylated moieties along a short PAA backbone. We showed that these OligoPEG ligands can easily promote the transfer of luminescent QDs and Au nanocrystals alike to buffer media, with excellent long-term stability of both sets of nanocrystals over a broad range of pHs and in the presence of added excess electrolytes. Furthermore, the ability to introduce different functional groups (such as N_3 and NH_2) into the oligomers opens the opportunity for orthogonal coupling of these nanocrystals to target biomolecules such as proteins and peptides, providing biologically active particle platforms for use in imaging and sensing.

dx.doi.org/10.1021/la203968t | Langmuir 2012, 28, 2761−2772

Combined, our results clearly confirm that higher ligand affinity to the nanocrystal surfaces (via increased thiol coordination number) produces substantial enhancement in colloidal stability for AuNPs and CdSe–ZnS QDs alike. Our design combines tunable multicoordination, hydrophilicity, reduced nonspecific interactions via adjustable PEG moieties, and reactivity, all in the same oligomer.[35,41,59] These observations open up a whole range of opportunities to couple different biological molecules with specific properties and functions to QDs and AuNPs and use them as platforms for sensing and imaging.

It is important to note that these ligands also permit the dispersion of these nanocrystals in several polar organic solvents such as methanol and ethanol. Moreover, this design can be easily extended to assemble custom-designed OligoPEG ligands with selective affinity to other homogeneous or hybrid inorganic nanocrystals such as those exhibiting magnetic properties. For example, we have recently prepared, characterized, and used dopamine-appended PEGylated oligomers and used them for cap-exchanging iron oxide nanoparticles and promoting their transfer to buffer media.[67]

■ ASSOCIATED CONTENT

Supporting Information

Additional experimental details on cap exchange of AuNPs, stability of QDs in growth media, the methyl-substituted maleimide synthesis, and peptide labeling with the dye. This material is available free of charge via the Internet at http://pubs.acs.org.

■ AUTHOR INFORMATION

Corresponding Author

*E-mail: mattoussi@chem.fsu.edu.

■ ACKNOWLEDGMENTS

The authors thank FSU, the National Science Foundation, and Pfizer for financial support. H.B.N. was supported by a fellowship from the National Research Foundation of Korea (D00074). The authors also thank Xin Ji and Suraj Dixit for their help regarding synthesis. We also thank Lei Bruschweiler for assistance with the gel experiments.

■ REFERENCES

(1) Alivisatos, A. P. *Science* **1996**, *271*, 933.
(2) Murray, C. B.; Kagan, C. R.; Bawendi, M. G. *Annu. Rev. Mater. Sci.* **2000**, *30*, 545.
(3) Klimov, V. I.; Mikhailovsky, A. A.; Xu, S.; Malko, A.; Hollingsworth, J. A.; Leatherdale, C. A.; Eisler, H. J.; Bawendi, M. G. *Science* **2000**, *290*, 314.
(4) Malko, A. V.; Mikhailovsky, A. A.; Petruska, M. A.; Hollingsworth, J. A.; Htoon, H.; Bawendi, M. G.; Klimov, V. I. *Appl. Phys. Lett.* **2002**, *81*, 1303.
(5) Nozik, A. J.; Beard, M. C.; Luther, J. M.; Law, M.; Ellingson, R. J.; Johnson, J. C. *Chem. Rev.* **2010**, *110*, 6873.
(6) Li, L.; Yang, X. C.; Gao, J. J.; Tian, H. N.; Zhao, J. Z.; Hagfeldt, A.; Sun, L. C. *J. Am. Chem. Soc.* **2011**, *133*, 8458.
(7) Chen, C. Y.; Cheng, C. T.; Lai, C. W.; Wu, P. W.; Wu, K. C.; Chou, P. T.; Chou, Y. H.; Chiu, H. T. *Chem. Commun.* **2006**, 263.
(8) Raymo, F. M.; Yildiz, I. *Phys. Chem. Chem. Phys.* **2007**, *9*, 2036.
(9) Medintz, I. L.; Uyeda, H. T.; Goldman, E. R.; Mattoussi, H. *Nat. Mater.* **2005**, *4*, 435.
(10) Michalet, X.; Pinaud, F. F.; Bentolila, L. A.; Tsay, J. M.; Doose, S.; Li, J. J.; Sundaresan, G.; Wu, A. M.; Gambhir, S. S.; Weiss, S. *Science* **2005**, *307*, 538.
(11) Biju, V.; Itoh, T.; Ishikawa, M. *Chem. Soc. Rev.* **2010**, *39*, 3031.
(12) Zrazhevskiy, P.; Sena, M.; Gao, X. H. *Chem. Soc. Rev.* **2010**, *39*, 4326.
(13) Pinaud, F.; Clarke, S.; Sittner, A.; Dahan, M. *Nat. Methods* **2010**, *7*, 275.
(14) Mattoussi, H., Cheon, J., Eds. *Inorganic Nanoprobes for Biological Sensing and Imaging*; Artech House: Norwood, MA, 2009.
(15) Jaiswal, J. K.; Mattoussi, H.; Mauro, J. M.; Simon, S. M. *Nat. Biotechnol.* **2003**, *21*, 47.
(16) Gao, X. H.; Cui, Y. Y.; Levenson, R. M.; Chung, L. W. K.; Nie, S. M. *Nat. Biotechnol.* **2004**, *22*, 969.
(17) Henglein, A. *Ber. Bunsen-Ges. Phys. Chem.* **1982**, *86*, 301.
(18) Rossetti, R.; Ellison, J. L.; Gibson, J. M.; Brus, L. E. *J. Chem. Phys.* **1984**, *80*, 4464.
(19) Murray, C. B.; Norris, D. J.; Bawendi, M. G. *J. Am. Chem. Soc.* **1993**, *115*, 8706.
(20) (a) Hines, M. A.; Guyot-Sionnest, P. *J. Phys. Chem.* **1996**, *100*, 468. (b) Dabbousi, B. O.; Rodriguez-Viejo, J.; Mikulec, F. V.; Heine, J. R.; Mattoussi, H.; Ober, R.; Jensen, K. F.; Bawendi, M. G. *J. Phys. Chem. B* **1997**, *101*, 9463.
(21) Peng, Z. A.; Peng, X. G. *J. Am. Chem. Soc.* **2001**, *123*, 183.
(22) Rogach, A.; Kershaw, S. V.; Burt, M.; Harrison, M. T.; Kornowski, A.; Eychmuller, A.; Weller, H. *Adv. Mater.* **1999**, *11*, 552.
(23) Rogach, A. L.; Kornowski, A.; Gao, M.; Eychmüller, A.; Weller, H. *J. Phys. Chem. B* **1999**, *103*, 3065.
(24) Allen, P. M.; Bawendi, M. G. *J. Am. Chem. Soc.* **2008**, *130*, 9240.
(25) Pons, T.; Pic, E.; Lequeux, N.; Cassette, E.; Bezdetnaya, L.; Guillemin, F.; Marchal, F.; Dubertret, B. *ACS Nano* **2010**, *4*, 2531.
(26) van Embden, J.; Jasieniak, J.; Mulvaney, P. *J. Am. Chem. Soc.* **2009**, *131*, 14299.
(27) Turkevich, J.; Stevenson, P. C.; Hillier, J. *Discuss. Faraday Soc.* **1951**, *11*, 55.
(28) Frens, G. *Nature (London), Phys. Sci.* **1973**, *241*, 20.
(29) Bruchez, M.; Moronne, M.; Gin, P.; Weiss, S.; Alivisatos, A. P. *Science* **1998**, *281*, 2013.
(30) Gerion, D.; Pinaud, F.; Williams, S. C.; Parak, W. J.; Zanchet, D.; Weiss, S.; Alivisatos, A. P. *J. Phys. Chem. B* **2001**, *105*, 8861.
(31) Hu, S.-H.; Gao, X. H. *Adv. Funct. Mater.* **2010**, *20*, 3721.
(32) Dubertret, B.; Skourides, P.; Norris, D. J.; Noireaux, V.; Brivanlou, A. H.; Libchaber, A. *Science* **2002**, *298*, 1759.
(33) Pellegrino, T.; Manna, L.; Kudera, S.; Liedl, T.; Koktysh, D.; Rogach, A. L.; Keller, S.; Rädler, J.; Natile, G.; Parak, W. J. *Nano Lett.* **2004**, *4*, 703.
(34) Carion, O.; Mahler, B.; Pons, T.; Dubertret, B. *Nat. Protoc.* **2007**, *2*, 2383.
(35) Yu, W. W.; Chang, E.; Falkner, J. C.; Zhang, J.; Al-Somali, A. M.; Sayes, C. M.; Johns, J.; Drezek, R.; Colvin, V. L. *J. Am. Chem. Soc.* **2007**, *129*, 2871.
(36) Lees, E. E.; Nguyen, T.-L.; Clayton, A. H. A.; Mulvaney, P. *ACS Nano* **2009**, *3*, 1121.
(37) Kim, S.-W.; Kim, S.; Tracy, J. B.; Jasanoff, A.; Bawendi, M. G. *J. Am. Chem. Soc.* **2005**, *127*, 4556.
(38) Wu, X.; Liu, H.; Liu, J.; Haley, K. N.; Treadway, J. A.; Larson, J. P.; Ge, N.; Peale, F.; Bruchez, M. P. *Nat. Biotechnol.* **2003**, *21*, 41.
(39) Mattoussi, H.; Mauro, J. M.; Goldman, E. R.; Anderson, G. P.; Sundar, V. C.; Mikulec, F. V.; Bawendi, M. G. *J. Am. Chem. Soc.* **2000**, *122*, 12142.
(40) Susumu, K.; Uyeda, H. T.; Medintz, I. L.; Pons, T.; Delehanty, J. B.; Mattoussi, H. *J. Am. Chem. Soc.* **2007**, *129*, 13987.
(41) Liu, W.; Howarth, M.; Greytak, A. B.; Zheng, Y.; Nocera, D. G.; Ting, A. Y.; Bawendi, M. G. *J. Am. Chem. Soc.* **2008**, *130*, 1274.
(42) Susumu, K.; Mei, B. C.; Mattoussi, H. *Nat. Protoc.* **2009**, *4*, 424.
(43) Jung, J.; Solanki, A.; Memoli, K. A.; Kamei, K.-I.; Kim, H.; Drahl, M. A.; Williams, L. J.; Tseng, H.-R.; Lee, K.-B. *Angew. Chem., Int. Ed.* **2010**, *49*, 103.
(44) Liu, W.; Greytak, A. B.; Lee, J.; Wong, C. R.; Park, J.; Marshall, L. F.; Jiang, W.; Curtin, P. N.; Ting, A. Y.; Nocera, D. G.; Fukumura, D.; Jain, R. K.; Bawendi, M. G. *J. Am. Chem. Soc.* **2010**, *132*, 472.

(45) Lee, J. H.; Huh, Y. M.; Jun, Y.; Seo, J.; Jang, J.; Song, H. T.; Kim, S.; Cho, E. J.; Yoon, H. G.; Suh, J. S.; Cheon, J. *Nat. Med.* **2007**, *13*, 95.
(46) Thomas, C. R.; Ferris, D. P.; Lee, J. H.; Choi, E.; Cho, M. H.; Kim, E. S.; Stoddart, J. F.; Shin, J. S.; Cheon, J.; Zink, J. I. *J. Am. Chem. Soc.* **2010**, *132*, 10623.
(47) Stewart, M. H.; Susumu, K.; Mei, B. C.; Medintz, I. L.; Delehanty, J. B.; Blanco-Canosa, J. B.; Dawson, P. E.; Mattoussi, H. *J. Am. Chem. Soc.* **2010**, *132*, 9804.
(48) Muro, E.; Pons, T.; Lequeux, N.; Fragola, A.; Sanson, N.; Lenkei, Z.; Dubertret, B. *J. Am. Chem. Soc.* **2010**, *132*, 4556.
(49) Lees, E. E.; Gunzburg, M. J.; Nguyen, T.-L.; Howlett, G. J.; Rothacker, J.; Nice, E. C.; Clayton, A. H. A.; Mulvaney, P. *Nano Lett.* **2008**, *8*, 2883.
(50) Bhang, S. H.; Won, N.; Lee, T.-J.; Jin, H.; Nam, J.; Park, J.; Chung, H.; Park, H.-S.; Sung, Y.-E.; Hahn, S. K.; Kim, B.-S.; Kim, S. *ACS Nano* **2009**, *3*, 1389.
(51) Liu, L.; Guo, X.; Li, Y.; Zhong, X. *Inorg. Chem.* **2010**, *49*, 3768.
(52) Yildiz, I.; McCaughan, B.; Cruickshank, S. F.; Callan, J. F.; Raymo, F. M. *Langmuir* **2009**, *25*, 7090.
(53) Yildiz, I.; Deniz, E.; McCaughan, B.; Cruickshank, S. F.; Callan, J. F.; Raymo, F. M. *Langmuir* **2010**, *26*, 11503.
(54) Shen, H. Y.; Jawaid, A. M.; Snee, P. T. *ACS Nano* **2009**, *3*, 915.
(55) Clapp, A. R.; Goldman, E. R.; Mattoussi, H. *Nat. Protoc.* **2006**, *1*, 1258.
(56) Qu, L. H.; Peng, Z. A.; Peng, X. G. *Nano Lett.* **2001**, *1*, 333.
(57) Mei, B. C.; Susumu, K.; Medintz, I. L.; Delehanty, J. B.; Mountziaris, T. J.; Mattoussi, H. *J. Mater. Chem.* **2008**, *18*, 4949.
(58) Uyeda, H. T.; Medintz, I. L.; Jaiswal, J. K.; Simon, S. M.; Mattoussi, H. *J. Am. Chem. Soc.* **2005**, *127*, 3870.
(59) Anderson, R. E.; Chan, W. C. W. *ACS Nano* **2008**, *2*, 1341.
(60) Choi, C. H. J.; Alabi, C. A.; Webster, P.; Davis, M. E. *Proc. Natl. Acad. Sci. U.S.A.* **2010**, *107*, 1235.
(61) Bullen, C.; Mulvaney, P. *Langmuir* **2006**, *22*, 3007.
(62) Munro, A. M.; Jen-La Plante, I.; Ng, M. S.; Ginger, D. S. *J. Phys. Chem. C* **2007**, *111*, 6220.
(63) Mei, B. C.; Oh, E.; Susumu, K.; Farrell, D.; Mountziaris, T. J.; Mattoussi, H. *Langmuir* **2009**, *25*, 10604.
(64) Lakowicz, J. R. *Principles of Fluorescence Spectroscopy*, 2nd ed.; Kluwer Academic/Plenum: New York, 1999.
(65) Clapp, A. R.; Medintz, I. L.; Mauro, J. M.; Fisher, B. R.; Bawendi, M. G.; Mattoussi, H. *J. Am. Chem. Soc.* **2004**, *126*, 301.
(66) Medintz, I. L.; Clapp, A. R.; Brunel, F. M.; Tiefenbrunn, T.; Uyeda, H. T.; Chang, E. L.; Deschamps, J. R.; Dawson, P. E.; Mattoussi, H. *Nat. Mater.* **2006**, *5*, 581.
(67) Na, H. B.; Palui, G.; Rosenberg, J. T.; Ji, X.; Grant, S. C.; Mattoussi, H. *ACS Nano* **2012**, DOI: 10.1021/nn203735b.